On the Retrieval of Sea Ice Thickness and Snow Depth using Concurrent Laser Altimetry and L-Band Remote Sensing Data

Lu Zhou[1], Shiming Xu[1], Jiping Liu[2], and Bin Wang[1,3]

[1]Ministry of Education Key Laboratory for Earth System Modeling, Department of Earth System Science, Tsinghua University, Beijing, China
[2]Department of Atmospheric and Environmental Sciences, University at Albany, State University of New York, Albany, NY, USA
[3]State Key Laboratory of Numerical Modeling for Atmospheric Sciences and Geophysical Fluid Dynamics (LASG), Institute of Atmospheric Physics, Chinese Academy of Sciences, Beijing, China

Correspondence to: Shiming Xu (xusm@tsinghua.edu.cn)

Abstract. The accurate knowledge of sea ice parameters, including sea ice thickness and snow depth over the sea ice cover, are key to both climate studies and data assimilation in operational forecasts. Large-scale active and passive remote sensing is the basis for the estimation of these parameters. In traditional altimetry or the retrieval of snow depth with passive microwave sensing, although the sea ice thickness and the snow depth are closely related, the retrieval of one parameter is usually carried out under assumptions over the other. For example, climatological snow depth data or as derived from reanalyses contain large or unconstrained uncertainty, which result in large uncertainty in the derived sea ice thickness and volume. In this study, we explore the potential of combined retrieval of both sea ice thickness and snow depth using the concurrent active altimetry and passive microwave remote sensing of the sea ice cover. Specifically, laser altimetry and L-band passive remote sensing data are combined using two forward models: the L-band radiation model and the isostatic relationship based on buoyancy model. Since the laser altimetry usually features much higher spatial resolution than L-band data from Soil Moisture Ocean Salinity (SMOS) satellite, there is potentially covariability between the observed snow freeboard by altimetry and the retrieval target of snow depth on the spatial scale of altimetry samples. Statistically significant correlation is discovered based on high-resolution observations from Operation IceBridge (OIB), and with a nonlinear fitting the covariability is incorporated in the retrieval algorithm. By using fitting parameters derived from large-scale surveys, the retrievability is greatly improved, as compared with the retrieval that assumes flat snow cover (i.e., no covariability). Verifications with OIB data show good match between the observed and the retrieved parameters, including both sea ice thickness and snow depth. With detailed analysis, we show that the error of the retrieval mainly arises from the difference between the modeled and the observed (SMOS) L-band brightness temperature (TB). The narrow swath and the limited coverage of the sea ice cover by altimetry is the potential source of error associated with the modeling of L-band TB and retrieval. The proposed retrieval algorithm (or methodology) can be applied to the basin-scale retrieval of sea ice thickness and snow depth, using concurrent passive remote sensing and active laser altimetry based on satellites such as ICESat-2 and WCOM.

Copyright statement. TEXT

1 Introduction

Sea ice is an important factor in the global climate system, playing key roles in modulating atmosphere and ocean interaction in the polar regions, the radiation budget through albedo effects, the ocean circulation through salinity and freshwater distribution (Screen and Simmonds, 2010; McPhee et al., 2009; Kurtz et al., 2011; Perovich et al., 2011). In the last decades, there has been rapid shrinkage of Arctic sea ice cover (Rothrock et al., 1999; Comiso et al., 2008; Stroeve et al., 2012; Laxon et al., 2013; Stocker et al., 2013), particularly in summer. In addition, the Arctic sea ice is also experiencing dramatic thinning in recent years (Kwok et al., 2009; Laxon et al., 2013), with the transition to overall younger sea ice age. Besides, the snow as accumulated over the sea ice cover also plays important roles due to its higher albedo as compared with sea ice, as well as thermal insulation which further hinders atmosphere-ocean interaction. With respect to changes in the sea ice cover, there is also significant decrease of the snow depth over the sea ice cover in the Arctic (Webster et al., 2014) which bears great deviation from climatology (Warren et al., 1999), indicating changes in the hydrological cycles such as late accumulation due to late freeze onset. The accurate knowledge of the sea ice cover and the snow over the sea ice, is key to the understanding of related scientific questions in climate change, as well as operational usage such as seasonal forecast.

The basin-scale observation of the sea ice cover mainly relies on satellite based remote sensing. Among the various sea ice parameters based on satellite retrieval, the most established is the sea ice concentration (or coverage). Figure 1 shows the various parameters related to satellite based laser altimetry and (L-band) passive radiometry for the sea ice cover. Passive microwave remote sensing of both Arctic and Antarctic is the basis of the retrieval of sea ice extent, with near realtime coverage since about 1979 based on satellite campaigns such as Scanning Multichannel Microwave Radiometer (SMMR), the Special Sensor Microwave/Imager (SSM/I) (Cavalieri et al., 1999), AMSR-E (Comiso et al., 2003), AMSR2 (Toudal Pedersen et al., 2017). However, the sea ice thickness is generally not retrievable through passive remote sensing techniques due to the saturation of radiative properties especially for high frequency ranges such as SMMR or SSM/I. In situ measurements of ice thickness through moored upward-looking sonar instruments and electromagnetic induction sounders mounted on sledges, ships, or helicopters/airplanes can provide sea ice thickness at specific locations or cross sections (Stroeve et al., 2014), so they are limited in terms of spatial coverage. Active remote sensing of satellite altimetry measures the overall height of the sea surface, serving as the major approach for the thickness retrieval of the sea ice. For radar altimetry, it is usually assumed that the radar signals penetrate the snow cover, and the main reflectance plane is the sea ice-snow interface (Laxon et al., 2003, 2013). Therefore in radar altimetry, the sea ice freeboard is measured. The sea ice thickness can be retrieved under certain estimation of the snow loading, such as climatological snow depth data in Warren et al. (1999) for multi-year sea ice (MYI) and halved for the first-year sea ice (FYI). Besides, for laser altimetry as in ICESat (Kwok and Cunningham, 2008; Kwok et al., 2009), the main reflectance surface is the snow-air interface, and the directly retrieved value is actually the snow (or total) freeboard. The snow loading is also required for the conversion of the snow freeboard to the sea ice thickness. As analyzed in Tilling et al.

(2015) and Zygmuntowska et al. (2014), the uncertainty in snow depth is the most important contributor to that of the sea ice thickness and volume.

The major reason of the uncertainty in snow depth and the loading on the sea ice cover is the lack of stable product for snow depth over the sea ice with good temporal and spatial coverage. The snow data as used in ICESat (Kwok and Cunningham, 2008) is derived from reanalysis data and satellite retrieved sea ice motion, while the climatological snow depth data in Warren et al. (1999) as used by CryoSat-2 (Laxon et al., 2013) contains large uncertainty due to interpolation and interannual variability, and may not be adequate for the present day under the context of climate change (Kwok et al., 2011; Webster et al., 2014). The retrieval of snow depth with passive microwave satellite remote sensing has been carried out in various studies. In Comiso et al. (2003), multi-band data from AMSR-E are utilized, but only for FYI. Maaß et al. (2013b) explored the retrieval of snow depth over thick sea ice with L-band data from SMOS. SMOS provides full coverage of polar regions on a near real-time (daily) basis. It has great advantage over satellite altimetry which can only achieve basin coverage on the scale of about one month. However, the sea ice thickness is required for the retrieval. Besides, with the better penetration of L-band signal in the sea ice cover, it is also demonstrated that there is retrievability of thin sea ice thickness with L-band data, as in Kaleschke et al. (2010) and Tian-Kunze et al. (2014). Although airborne remote sensing methods have limited spatial and temporal coverage, campaigns such as NASA's Operation IceBridge (OIB) carry out high-resolution scanning of the sea ice cover (Kwok et al., 2011; Kurtz and Farrell, 2011; Kurtz et al., 2013; Brucker and Markus, 2013), and provide invaluable data that are organized into flight-track based segments of the sea ice cover. The data can be adopted for the analysis of the status and variability of the sea ice cover at fine scale, as well as basin-scale studies as in Webster et al. (2014).

In this article, we propose a new algorithm that achieves simultaneous retrieval of both sea ice thickness and snow depth, based on two observations: the L-band passive microwave remote sensing and the laser altimetry that measures total freeboard. The potential of retrieval of these parameters lies in that both observations (freeboard and L-band radiative properties) are decided by these sea ice parameters. Specifically, we use OIB data (sea ice thickness, snow depth and snow freeboard) and concurrent SMOS L-band brightness temperature (TB) to simulate the simultaneous retrieval. It is found that the covariability of snow depth and freeboard at the local scale can greatly affect the well-posedness of the retrieval problem, and it is crucially important to include such covariability in the retrieval algorithm. Based on both realistic retrieval scenarios and large-scale retrieval with OIB and SMOS data, we demonstrate that the proposed algorithm can simultaneously retrieve both sea ice thickness and snow depth, and the error in the retrieved parameters mainly arises from the discrepancy between the sea ice area that corresponds to the SMOS measurement and that scanned by OIB. In Section 2 we first introduce the data, the models and the protocol of combined retrieval. Detailed statistics of snow depth and the effects of covariability on retrievability is covered in Section 3. Based on the statistics, we propose the retrieval algorithm and carry out evaluation and analysis in Section 4. Section 5 summarizes the article and provides discussion of related topics and future work.

2 Data and Models

2.1 Data

In order to construct and evaluate the retrieval algorithm, we mainly utilize two datasets, SMOS and OIB. SMOS measures the microwave radiation emitted from the Earth's surface in L-band (1.4GHz). In this article, we adopt the L3B TB product from SMOS. The daily gridded SMOS TB data field is generated from multiple snapshots within a day, with each snapshot involving multiple incident angles (ranging from 0 ° to 40 °) and spatially varying gain. The data is provided on the Equal-Area Scalable Earth (EASE) grid with a grid resolution of 12.5 km. However, due to the limitation of the satellite's antenna size, the effective resolution of L-band radiometer onboard SMOS is about 40 km.

High-resolution airborne remote sensing of sea ice parameters are available from OIB missions, starting in 2009 and covering western Arctic during winter months (mainly around March). This paper utilizes OIB measurements from 2012 to 2015, during which the measurements include surface temperature of the sea ice cover. The product is organized into tracks, and includes along-track measurements of total freeboard, surface temperature, snow depth. Due to the nature of the airborne measurements, the observations are limited to a narrow swath on the order of 100 m. Snow freeboard products are produced from Airborne Topographic Mapper (ATM) laser altimeter (Krabill and B., 2009). Sea ice thickness is retrieved from snow freeboard and snow depth, which is measured by the University of Kansas' snow radar (Leuschen, 2014). Surface temperature is determined from the IceBridge KT-19 infrared radiation pyrometer data set (Shetter et al., 2010). There is also accompanying sea ice type information, which is from Norwegian Meteorology Service OSI SAF system (Aaboe et al., 2016). Therein, the OIB Level-4 product IDCSI4 is adopted (Kurtz et al., 2013) for 2012-2013 and the remaining OIB data for 2014-2015 is from IDCSI2 Quicklook product, which is also available at NSIDC DAAC. Both of these two datasets are 40 m in resolution along the track's direction.

2.2 Data usage protocols

Due to the difference between OIB and SMOS data in both temporal and spatial coverage, we outline the following protocols of using the two data sets. OIB and SMOS data from the same day are taken. Spatially, for each OIB flight track, we locate all the EASE grids that contain OIB measurements. Figure 2 shows a typical case. Since OIB measurements are of a small swath, we consider the OIB data (of 40 m resolution) are samples of the underlying sea ice cover that contributes to a single SMOS TB measurement. However, due to the inherent resolution of SMOS is about 40 km and the daily gridded field is used in this study, we approximate the correspondence of OIB and SMOS TB by considering OIB measurements in the adjacent 3×3 cells (the red segment in Figure 2) of equal contribution to the SMOS TB at the central cell (the one bounded by thick blue lines in Figure 2). In total, the 9 cells cover an area of about 37.5 km × 37.5 km, which is coherent with the physical resolution of SMOS data.

It is worth noting that the area as covered by a single scan of the OIB track consists of less than 5 % of the total area that contributes to the SMOS TB. Therefore, we only treat the OIB data as samples of the underlying sea ice cover. The OIB sample count (denoted M) ranges from several hundreds to over 1000. The mean value of M is about 700, but there exists certain

areas with extensive scanning, which corresponds to a large value of M. Figure S2 shows the distribution of M for all available OIB data.

In order to exclude the potential effect of insufficient sampling or the inhomogeneity of the sea ice cover, we further exclude the following data for the analysis and evaluation. First, if an area is under-sampled by OIB (M <100), it is not considered for further analysis. Second, we exclude the cases in which a single SMOS TB corresponds to OIB samples with different sea ice types (i.e., mixed MYI and FYI). Third, we also exclude the cases involving sea ice leads as detected by the sea ice lead map in Willmes and Heinemann (2015a) or sea ice concentration lower than 1 according to Cavalieri et al. (1996). The purpose of these treatments is to rule out the factors that may compromise the quality of the OIB samples and allow focus on the discussion of the retrieval algorithm.

The snow freeboard as measured by OIB and the SMOS TB are used for the retrieval. The mean snow depth and mean sea ice thickness as measured by OIB are used for verification of the retrieval. Besides, since we assume the underlying sea ice cover as homogeneous within the retrieval scale (within 9 cells) and treat OIB measurements as samples to it, we also use the M measurements of snow depth to study the statistics of the snow depth and its covariability with snow freeboard.

2.3 L-band radiation model

The L-band (1.4 GHz) radiative property of the sea ice cover is characterized through numerical modeling based on Burke et al. (1979). The model was originally designed for the modeling of radiative transfer of the X- and L-band soil moisture. In Maaß et al. (2013b), this model is applied to sea ice and further used for the retrieval of snow depth over thick sea ice. In these works, a simple 1-layer formulation is used for both the sea ice and the snow cover over it. In order to better characterize the radiative properties of the sea ice, in this article we use a multi-layer formulation of the model with sea-ice type dependent vertical salinity and temperature profile (Zhou et al., 2017). The temperature profile in the vertical direction is linear in either the snow cover and the sea ice, assuming homogeneous thermal conductivity within the snow or the sea ice. Therefore the temperature in each sea ice or snow layer can be fully decided given the parameters of thermal conductivity, the ice bottom temperature (assumed to be -1.8 $^{\circ}C$), and the snow surface temperature. The salinity profile of FYI differs from that of MYI. For FYI, the salinity of all layers of the sea ice all equals the bulk salinity, which decreases with the sea ice thickness. For MYI, a surface-drained profile is adopted to reflect the effect of summer melt and flushing. Figure 3.a shows the sea ice salinity profiles under the different sea ice types or thickness. The dielectric properties, the emissivity of the layers and the overall radiative properties of the sea ice cover is modeled, following Kaleschke et al. (2010) and Maaß et al. (2013a). The convergence of the modeled TB with respect to the layer count is witnessed, which is consistent with the study in Maaß et al. (2013a). In Zhou et al. (2017), it is demonstrated that the multi-layer treatment and the salinity profile MYI yields good fit between the simulated TB and SMOS TB. Part 1 of the supplementary material provides introduction to the details of the model, including the verification with OIB and SMOS data. Figure 3.c shows the modeled TB under typical sea ice parameters for MYI under typical winter Arctic conditions (surface temperature of -30 $^{\circ}C$). The green contour lines are constant FB_s lines. With the thickening of sea ice cover, the value of TB increases and saturates when hi is large enough (larger than 2.5 m). The value of TB is not monotonic with respect to FB_s, and for certain value combinations of snow freeboard and TB, two

solutions are possible. This results in the potential problem of ill-posedness for the retrieval with realistic observational data, as is discussed in Section 3.2.

In order to match the protocol of the SMOS TB data product, we also simulate the mean of horizontal and vertical polarization TB among 0 ° to 40 °. We consider the correspondence between a single SMOS TB value and the arithmetic mean of all the M TB values simulated by the radiation model using the M corresponding OIB samples (each with sea ice thickness, snow depth, surface temperature and sea ice type). Figure 3.b shows the comparison of modeled TB and SMOS TB, by using all available data. The least squares (LSQ) fit line (dashed line) and the LSQ fit line with the constraint that the slope be 1 (dotted line) are shown. The root mean square error (RMSE) in modeled TB as compared with SMOS data is about 3.1 K. The R^2 value for the second fit is 0.54 with an intercept of $-1.637K$, which is treated as a model bias and canceled in further studies. As noted in Section 2.2, there is potentially insufficient sampling of OIB data, so we further consider areas with more extensive OIB sampling. Specifically, cells with large values of sample count M (over 95 percentile) are considered to be more thoroughly scanned spatially, and the RMSE of TB for these cells drops to 1.41 K. Figure S3 shows the relationship between RMSE of TB to the value of M, which demonstrates that the lack of sufficient spatial coverage is an important source for the difference between the modeled TB and the SMOS observation. Based on the aforementioned RMSE of 1.41 K for well-surveyed regions, we only consider the retrieval for cells with an TB error within 1.5 K for further studies. In all 412 TB cells are available, containing 35 OIB tracks and 321'168 OIB measurements. They account for about 50% of all available TB cells. We consider this is a limitation of combined usage of OIB and SMOS data, and the retrieval with actual satellite laser altimetry and L-band TB can be free from this limitation through better altimetric scanning and wider swath as compared with OIB.

2.4 Isostatic equilibrium model

Apart from the L-band radiation model, the other model as used by the retrieval is the equilibrium model based on the buoyancy relationship. Under certain assumptions of the sea ice density (denoted ρ_{ice}), sea water density (denoted ρ_{water}) and snow density (denoted ρ_{snow}) and the equilibrium state, the sea ice thickness, snow depth and snow freeboard FB_s are constrained according to Equation 1. And the sea ice thickness can be derived given the snow depth, according to Equation 2. This model is widely applied for both radar and laser altimetry for the retrieval of sea ice thickness.

$$\rho_{ice} \cdot hi + \rho_{snow} \cdot hs = \rho_{water} \cdot (hi + hs - FB_s) \tag{1}$$

$$hi = \frac{\rho_{water}}{\rho_{water} - \rho_{ice}} \cdot FB_s - \frac{\rho_{water} - \rho_{snow}}{\rho_{water} - \rho_{ice}} \cdot hs \tag{2}$$

In this study, ρ_{water} and ρ_{ice} are taken to be 1024 kg/m^3 and $915 kg/m^3$ which are derived from field measurements discussed by Wadhams et al. (1992), and ρ_{snow} is 320 kg/m^3 derived from Warren et al. (1999).

3 Covariability between snow depth and snow freeboard and the effect on retrievability

We analyze the covariability between the snow depth (hs) and the snow freeboard (FB_s) on the scale of retrieval. Under the context of retrieval, we base the analysis with the freeboard measurements as a priori, and focus on how the snow depth changes with freeboard in a statistical sense. By using M available OIB samples that correspond to a single TB measurement, we show that there exists statistically significant correlation between the two data, and the relationship is better characterized by a nonlinear fitting. Furthermore, the effect of the covariability on retrievability is analyzed in Section 3.2.

3.1 Covariability analysis based on OIB data

For the covariability between FB_s and hs, we choose the native resolution of the OIB product (40 m) as the spatial scale for analysis. Each TB corresponds to multiple (M) OIB samples, with each sample containing the measurement for both FB_s and hs. We divide these samples into FB_s bins, with each bin covering 5 cm. In total there are 30 bins, covering the range of 0 to 1.5 m. For samples in each bin, we compute the percentiles and the mean value of hs. Figure 4.a shows the mean hs and the +/-1 standard deviation range and their relationship with FB_s, for 4 representative TB points. Furthermore, we carry out least squares fitting (weighted according to sample count in each bin) between mean hs and FB_s. Among all available TB and OIB data, there exist statistically significant positive correlation between hs and FB_s for over 90% of all points. The values of R^2 are in the range of 0.06 and 0.89 (95% percentile), with the mean value of R^2 as 0.53. This indicates that there exists consistent covariability between snow depth and snow freeboard across Arctic sea ice cover.

However, for both FYI and MYI ice, there is saturation of the mean snow depth with respect to the snow freeboard. Besides, in the Arctic inundation is generally uncommon (i.e., $hs < FB_s$). In order to accommodate these characteristics, we propose a nonlinear fitting as Equation 3. The parameters α and β are fitted according to observations which are both larger than 0. According to the equation, the value of hs saturates to $\alpha \cdot \pi/2$ with large values of FB_s, and the value of $\alpha \cdot \beta$ (denoted s) which is the slope of the function at $FB_s = 0$ should be lower than 1 in order to avoid inundation. Figure S4 and S5 (in part 2 of the supplementary material) show the statistics of α, β and s for FYI and MYI, respectively.

$$hs(FB_s) = \alpha \cdot \arctan(\beta \cdot FB_s) \tag{3}$$

Using Equation 3, the overall quality of the fitting for all available local OIB segments is improved, with mean value of R^2 rising from 0.53 to 0.67, and the 95% percentile of R^2 rises to 0.23 and 0.92 respectively. Based on statistics of all the available OIB data, the value of s for the local OIB segment is in the range of 0.49 and 0.96 (95% percentile) with a single mode distribution for both MYI and FYI (Figure S4.c and S5.c). For FYI, the mean value of s is 0.71 and for MYI 0.95, which implies a generally thicker snow cover over MYI. Among all the local OIB segments, 80% of them witnessed a value of s lower than 1.

We consider the value of s to be stable across either FYI or MYI sea ice, and choose these values as universal parameters for the design of the retrieval algorithm. Figure 4.b shows fitting function of snow depth over snow freeboard based on these representative values of s under various values for α.

3.2 Effects on retrievability

We evaluate the covariability and its effect on retrieval from several aspects. We choose 5 realistic retrieval scenarios among all the OIB and SMOS data, with two of them representing FYI retrieval, and three of them for MYI. As shown in Table 1, they represent typical retrieval problems for Arctic sea ice. Besides, the simulated TB values by the radiation model is close to the corresponding SMOS TB values (within 1.5 K). Based on these scenarios, we examine whether it is possible to retrieve the actual sea ice thickness and snow depth, with or without the covariability. Firstly we ignore the covariability, and assume a flat snow cover. For all the M OIB samples, we assume that the snow depth is uniform. For the retrieval problem, since the directly observed values are freeboard samples ($FB_s|_m$, where m is the index of the samples, and $1 \leq m \leq M$), we carry out the scanning of the (uniform) snow depth hs from 0 m (snow free) to 1 m. Under a certain value of hs, we retrieve the sea ice thickness $hi|_m$ for each $FB_s|_m$ with Equation 2, based on the current value of hs. Then the TB value for this sample ($TB|_m$) can be calculated according to the L-band radiation model, with $hi|_m$, hs and surface temperature $T_{sfc}|_m$. The mean TB value is then computed as the arithmetic mean of all $TB|_m$'s, for the current value of hs. For any sample of FB_s, if the value of freeboard is smaller than the current value of hs, in order to avoid inundation, the snow depth for this sample is assumed to be the same as FB_s.If the number of samples that witness potential of inundation over 50 % of M, we stop the scanning even if hs has not reached 1 m.

In order to incorporate the effect of covariability, we adopt either the global value of s (0.71 for FYI and 0.95 for MYI) or the locally fitted value of s and carry out the retrieval. Figure 5.a shows 4 typical distribution of FB_s, and Figure 5.b shows a range of values for α (0 to 1) and the resulting mean value of hs for the 4 typical distributions. For the range of 0 to 1, the resulting mean hs covers a continuous range for each distribution. For each distribution, when α is very small, the corresponding hs is very small for whole range FB_s, resulting in a very small value of mean hs. Furthermore, the value of mean hs approaches 0 when α approaches 0, which in effect corresponds to the “bare-snow" case. With the grow of α, there exists monotonous increase in the mean hs, and when α is large enough, the mean hs saturates. For all of the 4 FB_s distributions, we consider that the resulting mean hs is reasonable for the range of α. Therefore, the retrieval of snow depth is attained by locating the proper value of α. Due to the potential of double solution in the retrieval, the solving of α is attained by a scanning process that cover the reasonable range for α. The scan starts from 0.001, steps by 0.01, and it is limited to a large value that yields saturation for mean hs. With each scanned value of α, a corresponding value for β can be computed as s/α, and the snow depth $hs|_m$ for each sample can be computed with Equation 3. Then the $hi|_m$, the TB values for each sample can be computed, as well as the mean snow depth and mean TB.

We record the (mean) snow depth, and the corresponding mean TB across the scanning process. Figure 6 shows the results of scanning for the five scenarios in Table 1. Note that for the lines that represent scanning of α (i.e., involving covariability), the x-axis is the resulting values of mean hs, not α. The observed TB and the simulated TB (with OIB data) are shown by solid

and dot-dashed horizontal lines, respectively. Besides, the observed mean snow depth and the 50 % inundation with flat snow cover are shown by solid and dashed vertical lines, respectively. The simulated TB with flat snow cover (black dashed curve in each subfigure) is always lower than that with covariability information (blue dashed curves for results with global s and red ones for those with local s). For all the scenarios, the TB values that are attained through scanning can reach the observed TB with the incorporation of covariability, while with the flat snow cover assumption, the values of TB in two scenarios (III and IV) fail to reach the observation. This implies that with the flat snow cover assumption, there is no solution to the retrieval problem. We further examine the other 3 scenarios, the solutions of the retrieval problem reside at the crosspoint of the scanned TB curves and the horizontal bars that represent observational TB values. The solutions of mean snow depth under the flat snow cover assumption are always larger than the observed mean snow depth by over 5 cm.

For the comparison between the covariability incorporated scanning with local s and global s, we show that for scenario I, II, III and IV, the solutions of the two scanning are close to each other (within 2 cm). For Scenario II, III and IV, the solutions as produced by the scanning is close to the observed snow depth. The differences between the solutions produced by scanning and the observed snow depth are 5 cm or larger for scenario I and V, with the scanning with local s produces smaller errors. It is worth noting that for the actual retrieval process, the local value of s is not available, and only the global value of s is usable. Lastly, for scenario III, two potential solutions exist (two crossing points between the TB scanning curve and the observational TB). Without extra observational data during retrieval, it is not possible to judge which solution is the true (or better) one. Therefore the retrieval algorithm should be able to locate both possible solutions.

The covariability as observed with OIB data plays an important role in the retrievability of the sea ice parameters. Also with OIB data, we extract the statistical relationship (Equation 3) that characterizes the covariability which can be incorporated in the retrieval. However, during retrieval, the parameter s is generally not available for the local sea ice cover, and the global values of s (for FYI and MYI) as computed from high-resolution OIB data can be adopted.

4 Retrieval algorithm and evaluation

In order to incorporate the covariability characteristics, we design the retrieval algorithm for sea ice thickness and snow depth that include two distinctive phases. The covariability feature is based on the nonlinear fitting in Equation 3 and the fixed value of s for both FYI and MYI sea ice as derived from OIB data. The first phase involves the scanning of possible snow depth configurations. This phase is in effect carried out by the scanning of the value of α from 0.001 to 3 (or sufficiently large). A possible solution is detected between two adjacent values of α, when the TB values as generated with these two values of α are on the different side of the observed TB. During the second phase, all the possible solutions are then computed with an iterative binary search of α. All possible solutions are reported by the retrieval algorithm. The outline of the algorithm is presented in Figure 7, with the two phases marked out by red and blue boxes, respectively. We also construct a reference retrieval algorithm based on the flat snow cover assumption, for which the scanning is over the snow depth instead of α. The details of this reference algorithm is omitted for brevity. We carry out the evaluation from two aspects, the retrieval with typical scenarios as presented in Section 3.2, as well as large-scale retrieval with available OIB data.

For the typical scenarios, we carry out the retrieval for the mean sea ice thickness ($\overline{Hi}$) and the mean snow depth ($\overline{Hs}$) using the standard algorithm with both global and local values of s, as well as the reference algorithm. Table 2 shows the comparison of the retrieval results and observations. The reference algorithm (with flat snow cover assumption) consistently performed worse than the standard algorithm. For scenario I and IV, it even failed to attain any solution. For the standard algorithm, the use of local value of s usually results in small errors in both $\overline{Hi}$ and $\overline{Hs}$. Also for scenario III for which two solutions are possible, the retrieval algorithm addresses both of them. The retrieval results are consistent with the retrievability analysis in Section 3.2.

In order to verify the algorithm, we carry out the retrieval with all the available OIB data (as mentioned in Section 2.3) which are from 35 OIB tracks and 412 SMOS TB measurements, and correspond to 412 retrieval cases. For each SMOS TB, the corresponding samples (snow freeboard, surface temperature and sea ice type) which are from OIB dataset are used for the retrieval. The retrieval with the flat snow cover assumption (the reference algorithm) is only successful for 50 cases, which accounts for about 12 % of available cases. For comparison, the (standard) algorithm achieves retrieval for 391 cases (95%) with the global s values, and for all the TB values with the locally fit s values. Figure 8 shows the comparison of retrieved mean sea ice thickness and snow depth with observations. Figure 8.a and b shows the results for sea ice thickness and snow depth, based on: (1) simulated TB (as computed from the radiation model), and (2) the local value of s. This represent the most "ideal" retrieval case in which there exists no extra uncertainty. As shown in Figure 8.a, the LSQ fit for $\overline{Hi}$ (dash line) features a R^2 value of 0.966, while the LSQ fit under the extra constraint on slope (dotted dash line) features a R^2 value of 0.964. Also for snow depth (Figure 8.b), the R^2 values for the two fittings are both 0.844. This indicates that the retrieval is in good agreement with the observations.

For the actual retrieval problem for which the local value of s is unknown and the observational TB values from SMOS, Figure 8.c and d shows the evaluation for sea ice thickness and snow depth respectively. The fitting quality (in terms of R^2) for sea ice thickness is as high as 0.89 and that for snow depth is 0.637. It is worth noting that these results are achieved with only statistical data derived from large-scale OIB surveys. Furthermore, if the retrieval is based on: (1) observed TB from SMOS, and (2) the locally fitted value of s, the R^2 values for the fitting are 0.91 and 0.65 for sea ice thickness and snow depth respectively, with virtually no change in the fitting lines (not shown). There is minor increase in quality (0.91 versus 0.89 and 0.65 versus 0.637) and a relatively large gap to the "ideal" case. As a comparison, we also carry out retrieval with the TB with forward model and the local values of s, and the R^2 for fittings between the retrieved and the observed parameters for sea ice thickness and snow depth are 0.96 and 0.84, respectively. This indicates that the difference (or error) of the modeled and the observed TB plays an important role in affecting the quality of the retrieval. The uncertainty of TB may arise from that of the radiation model, as well as the mismatch between the altimetry and passive microwave remote sensing, as introduced in Section 2.2.

For comparison, we carry out comparison with the idealized scenario of retrieval which only involves TB and the mean value of FB_s. This idealized scenario in Xu et al. (2017) ignores the resolution difference between altimetry scans and L-band radiometry, and it represents a theoretical study of the retrieval problem. Specifically, for the use of OIB data, the mean value of M samples of FB_s is computed, and further combined with TB for the retrieval of a single value of sea ice thickness and

snow depth. Since only the mean FB_s is involved in the retrieval, covariability does not play a role in the retrieval. By using the same SMOS and OIB data as the evaluation in Figure 8, the retrieval yields R^2 of 0.78 and 0.50 for hi and hs (fitting between the retrieved and the observed parameter). For a comparison, under the realistic scenario which involves multiple altimetry scans for a single TB (Figure 8.c and d), the quality of retrieval is much improved for both hi (R^2 from 0.78 to 0.89) and hs (R^2 from 0.50 to 0.64). This demonstrates that the high-resolution altimetry samples and the accompanying covariability information play an important role in improving the retrieval, as compared with the idealized retrieval scenario in Xu et al. (2017).

Based on the retrieval with large-scale observational data, the proposed algorithm achieves effective retrieval of both sea ice thickness and snow depth, by using simultaneous remote sensing of the sea ice cover, i.e., laser altimetry and L-band passive microwave sensing. The statistics of snow depth and its covariability with snow freeboard on the spatial scale of retrieval plays an important role in improving the well-posedness of the retrieval problem, as well as the quality of the retrieved parameters.

5 Summary and discussion

In this study, we introduce a novel algorithm for retrieving multiple Arctic sea ice parameters based on combination of L-band passive microwave remote sensing and active laser altimetry. Two physical models, the L-band radiation model and the buoyancy relationship, are adopted to constrain the sea ice thickness and snow depth. They are used as forward models during an iterative retrieval process that solves the sea ice parameters that satisfy the observed L-band TB and snow freeboard values. Specifically, according to observations, there exists covariability between the snow depth and the snow freeboard which are the objective and the input for the retrieval, respectively. The covariability plays a key role in the retrievability, and therefore should be incorporated in the retrieval algorithm. A nonlinear fitting that characterizes the covariability is derived from OIB data, and a parameter (initial slope of the fitting function) is considered to be stable among large-scale observations. This set of parameters (for FYI and MYI respectively) is adopted in the retrieval algorithm. Verification with available OIB data shows that the retrieval is attained for both sea ice thickness and snow depth, with the uncertainty mainly arising from the mismatch between modeled and observed TB values. This algorithm can be applied to the large-scale retrieval of sea ice thickness and snow depth using concurrent L-band satellite remote sensing and satellite altimetry of the sea ice cover such as Abdalati et al. (2010).

There are key differences between the proposed algorithm with existing retrieval methods. In traditional (laser) satellite altimetry, the retrieval of sea ice thickness mainly relies on (adapted) climatological snow depth or data as derived from reanalyses, which may contain unconstrained uncertainty due to model biases as well as missing physical processes. Besides, these snow depth data usually lack fine-scale details that match the resolution of satellite altimetry, such as the covariability characteristics. On the other hand, the retrieval of snow depth using L-band SMOS data as in Maaß et al. (2013b) relies on the a priori knowledge of the thickness of the (thick) sea ice. Contrary to these existing retrieval algorithms, the proposed algorithm carries out retrieval of both sea ice thickness and snow depth, with the concurrent active and passive remote sensing of the sea

ice cover. Since no climatological snow depth or any other derived snow data is used in the algorithm, the retrieved sea ice thickness do not suffer from the potential lack of efficacy of these data.

In Kwok et al. (2011), statistical analyses are carried out between snow depth and snow freeboard, which also show covariability between the two. However, it is worth noting that the scale and the resolution as adopted in Kwok et al. (2011) are about 400 km and 4 km, respectively. They are both much larger than the those as used in this study (about 40 km and 40 m). While the analyses in Kwok et al. (2011) is on coarser spatial scales, our work focuses on the spatial scale that is relevant to the retrieval of sea ice parameters. We demonstrate that on this relatively small spatial scale, there still exists covariability between snow depth and snow freeboard.

The proposed retrieval method is the basis for the retrieval of sea ice parameters with data from concurrent satellite campaigns. Although there was no concurrent L-band satellite observation with the ICESat campaign, there are candidate satellite campaigns such as WCOM (Shi et al., 2016) that provides concurrent L-band observation with the planned ICESat-2 campaign. For the study with satellite data, there exist several practical issues. First, the snow surface temperature is provided by airborne sensors in OIB, but not generally available with laser altimetry. Several data sources serve as candidate data for the concurrent surface temperature field, such as reanalysis data (Dee et al., 2011), MODIS based product (Hall et al., 2004). Second, there exists small-scale variability of the sea ice cover such as leads, which were not considered for the analysis and verification in this study. As shown in Zhou et al. (2017), the presence of sea ice leads has profound effect in lowering the overall TB on the scale of SMOS observations. Leads can be treated as small-scale heterogeneity of the sea ice cover, and the incorporation of lead maps such as Willmes and Heinemann (2015b) effectively reduces the overestimation of TB, as studied in Zhou et al. (2017). Specifically, the lead map can be adopted by the retrieval through the integration with the forward radiation model. Other types of small scale variability such as mixture of FYI and MYI, should be also accounted for using sea ice type maps. Third, the covariability explored in this study is on the spatial scale of the original OIB data (i.e., 40 m). For each specific satellite altimetry, we consider the freeboard measurement the mean freeboard value within a certain spatial range. For ICESat-2, each laser scan dot covers a circular region of about 70 m in diameter (Abdalati et al., 2010). The scaling of the covariability should be studied for the specific resolution of the satellite altimetry. By using 70 m as the typical resolution of ICESat-2, we deduce the value of s at this resolution by manual coarsening OIB's data by averaging adjacent points. In effect, the value of s at 80 m is computed, which shows a slight decrease of s for both FYI and MYI. Figure S6 (in part 2 of the supplementary material) shows the general scaling of s for the resolution range from 40 m to 240 m. Fourth, in order to estimate the uncertainty of the retrieved parameters, the effects of surface temperature, as well as other data sources (including TB, freeboard measurements, and the value of s), should be evaluated in a systematic way. Due to the nonlinear relationship between TB and the sea ice parameters, Monte-Carlo simulations can be carried out for the quantification of the uncertainty. Besides, for the historical data from from ICESat (Kwok and Cunningham, 2008) during the first decade of the 21st century, due to the lack of basin-scale L-band observation for the Arctic, other passive remote sensing data such as C-band data from AMSR-2 can be exploited in a similar manner for the retrieval of these historical data.

Acknowledgements. This work is partially supported by National Key R & D Program of China under the grant number of 2017YFA0603902 and the General Program of National Science Foundation of China under the grant number of 41575076. The authors would like to thank the editors and referees for their invaluable efforts in improving the manuscript. SMOS data is provided from Integrated Climate Data Center (ICDC), icdc.cen.uni-hamburg.de, University of Hamburg, Germany, Digital media. http://icdc.cen.uni-hamburg.de/1/daten/cryosphere/l3b-smos-tb.html. [Data Accessed: 2017/10/25]. OIB and SSM/I sea ice concentration data are provided by NASA National Snow and Ice Data Center Distributed Active Archive Center, Boulder, Colorado USA. doi: http://dx.doi.org/10.5067/7XJ9HRV50O57. [Data Accessed: 2017/10/25]. Besides, the authors are grateful to Willmes, S. and Heinemann, G. for the provision of Arctic sea ice lead map.

References

Aaboe, S., Breivik, L.-A., Eastwood, S., and Sorensen, A.: Sea Ice Edge and Type Products, http://osisaf.met.no/p/ice/edge_type_long_description.html, accessed: 2016-12-30, 2016.

Abdalati, B., Zwally, H., Bindschadler, R., Csatho, B., Farrell, S., Fricker, H., Harding, D., Kwok, R., Lefsky, M., Markus, T., Marshak, A., Neumann, T., Palm, S., Schutz, B., Smith, B., Spinhirne, J., and Webb, C.: The ICESat-2 laser altimetry mission, in: Proc. IEEE, vol. 98, pp. 735–751, doi:10.1109/JPROC.2009.2034765, 2010.

Brucker, L. and Markus, T.: Arctic-scale assessment of satellite passive microwave-derived snow depth on sea ice using Operation IceBridge airborne data, Journal of Geophysical Research: Oceans, 118, 2892–2905, 2013.

Burke, W., Schmugge, T., and Paris, J.: Comparison of 2.8-and 21-cm microwave radiometer observations over soils with emission model calculations, Journal of Geophysical Research: Oceans, 84, 287–294, 1979.

Cavalieri, D., Parkinson, C., Gloersen, P., and Zwally, H.: Sea Ice Concentrations from Nimbus-7 SMMR and DMSP SSM/I-SSMIS Passive Microwave Data, Boulder, Colorado USA. NASA National Snow and Ice Data Center Distributed Active Archive Center. doi: http://dx.doi.org/10.5067/8GQ8LZQVL0VL., 1996.

Cavalieri, D. J., Parkinson, C. L., Gloersen, P., Comiso, J. C., and Zwally, H. J.: Deriving long-term time series of sea ice cover from satellite passive-microwave multisensor data sets, Journal of Geophysical Research: Oceans, 104, 15 803–15 814, 1999.

Comiso, J., Cavalieri, D., and Markus, T.: Sea ice concentration, ice temperature, and snow depth using AMSR-E data, IEEE Trans. Geosci. Remote Sens., 41, 243–252, 2003.

Comiso, J. C., Parkinson, C. L., Gersten, R., and Stock, L.: Accelerated decline in the Arctic sea ice cover, Geophysical research letters, 35, 2008.

Dee, D., Uppalaa, S., Simmonsa, A., Berrisforda, P., Polia, P., Kobayashib, S., Andraec, U., Balmasedaa, M., Balsamoa, G., Bauera, P., Bechtolda, P., Beljaarsa, A., van de Berg, L., Bidlota, J., Bormanna, N., Delsola, C., Dragania, R., Fuentesa, M., Geera, A., Haimbergere, L., Healya, S., Hersbacha, H., Holma, E., Isaksena, L., Kallbergc, P., Kohlera, M., Matricardia, M., McNallya, A., Monge-Sanzf, B., Morcrettea, J.-J., Parkg, B.-K., Peubeya, C., de Rosnaya, P., Tavolatoe, C., Thepauta, J.-N., and Vitart, F.: The ERA-Interim reanalysis: configuration and performance of the data assimilation system, Quarterly Journal of the Royal Meteorological Society, 137, 553–597, 2011.

Hall, D., Key, J., Casey, K., Riggs, G., and Cavalieri, D.: Sea ice surface temperature product from MODIS, IEEE T. Geosci. Remote, 42, 1076–1087, 2004.

Kaleschke, L., Maaß, N., Haas, C., Hendricks, S., Heygster, G., and Tonboe, R.: A sea-ice thickness retrieval model for 1.4 ghz radiometry and application to airborne measurements over low salinity sea-ice, The Cryosphere, 4, 583–592, 2010.

Krabill and B., W.: IceBridge ATM L1B Qfit Elevation and Return Strength, [indicate subset used], Boulder, Colorado USA: NASA DAAC at the National Snow and Ice Data Center. http://dx.doi.org/10.5067/DZYN0SKIG6FB, updated 2013, 2009.

Kurtz, N., Markus, T., Farrell, S., Worthen, D., and Boisvert, L.: Observations of recent Arctic sea ice volume loss and its impact on ocean-atmosphere energy exchange and ice production, Journal of Geophysical Research: Oceans, 116, 2011.

Kurtz, N. T. and Farrell, S. L.: Large-scale surveys of snow depth on Arctic sea ice from Operation IceBridge, Geophysical Research Letters, 38, doi:10.1029/2011GL049216, http://dx.doi.org/10.1029/2011GL049216, l20505, 2011.

Kurtz, N. T., Farrell, S. L., Studinger, M., Galin, N., Harbeck, J. P., Lindsay, R., Onana, V. D., Panzer, B., and Sonntag, J. G.: Sea ice thickness, freeboard, and snow depth products from Operation IceBridge airborne data, The Cryosphere, 7, 1035–1056, doi:10.5194/tc-7-1035-2013, www.the-cryosphere.net/7/1035/2013/, 2013.

Kwok, R. and Cunningham, G. F.: ICESat over Arctic sea ice: Estimation of snow depth and ice thickness, Journal of Geophysical Research: Oceans, 113, doi:10.1029/2008JC004753, http://dx.doi.org/10.1029/2008JC004753, c08010, 2008.

Kwok, R., Cunningham, G. F., Wensnahan, M., Rigor, I., Zwally, H. J., and Yi, D.: Thinning and volume loss of the Arctic Ocean sea ice cover: 2003-2008, Journal of Geophysical Research: Oceans, 114, doi:10.1029/2009JC005312, http://dx.doi.org/10.1029/2009JC005312, c07005, 2009.

Kwok, R., Panzer, B., Leuschen, C., Pang, S., Markus, T., Holt, B., and Gogineni, S.: Airborne surveys of snow depth over Arctic sea ice, Journal of Geophysical Research: Oceans, 116, 2011.

Laxon, S., Peacock, N., and Smith, D.: High interannual variability of sea ice thickness in the Arctic region, Nature, 425, 947, 2003.

Laxon, S. W., Giles, K. A., Ridout, A. L., Wingham, D. J., Willatt, R., Cullen, R., Kwok, R., Schweiger, A., Zhang, J., Haas, C., Hendricks, S., Krishfield, R., Kurtz, N., Farrell, S., and Davidson, M.: CryoSat-2 estimates of Arctic sea ice thickness and volume, Geophysical Research Letters, 40, 732–737, doi:10.1002/grl.50193, 2013.

Leuschen, C.: IceBridge Snow Radar L1B Geolocated Radar Echo Strength Profiles, Version 2. [Indicate subset used], Boulder, Colorado USA. NASA National Snow and Ice Data Center Distributed Active Archive Center. doi: http://dx.doi.org/10.5067/FAZTWP500V70, updated 2017, 2014.

Maaß, N., Kaleschke, L., and Stammer, D.: Remote sensing of sea ice thickness using SMOS data, Ph.D. thesis, University of Hamburg Hamburg, 2013a.

Maaß, N., Kaleschke, L., Tian-Kunze, X., and Drusch, M.: Snow thickness retrieval over thick Arctic sea ice using SMOS satellite data, The Cryosphere, 7, 1971–1989, doi:10.5194/tc-7-1971-2013, www.the-cryosphere.net/7/1971/2013/, 2013b.

McPhee, M., Proshutinsky, A., Morison, J. H., Steele, M., and Alkire, M.: Rapid change in freshwater content of the Arctic Ocean, Geophysical Research Letters, 36, 2009.

Perovich, D., Jones, K., Light, B., Eicken, H., Markus, T., Stroeve, J., and Lindsay, R.: Solar partitioning in a changing Arctic sea-ice cover, Annals of Glaciology, 52, 192–196, 2011.

Rothrock, D. A., Yu, Y., and Maykut, G. A.: Thinning of the Arctic sea-ice cover, Geophysical Research Letters, 26, 3469–3472, 1999.

Screen, J. A. and Simmonds, I.: The central role of diminishing sea ice in recent Arctic temperature amplification, Nature, 464, 1334, 2010.

Shetter, R., Buzay, E., and Gilst., D. V.: IceBridge NSERC L1B Geolocated Meteorologic and Surface Temperature Data, Version 1. [Indicate subset used]., Boulder, Colorado USA. NASA National Snow and Ice Data Center Distributed Active Archive Center. doi: http://dx.doi.org/10.5067/Y6SQDAAAOEQU., updated 2013, 2010.

Shi, J., Dong, X., Zhao, T., Du, Y., Liu, H., Wang, Z., Zhu, D., Ji, D., Xiong, C., and Jiang, L.: The water cycle observation mission (WCOM): Overview, in: 2016 IEEE International Geoscience and Remote Sensing Symposium (IGARSS), pp. 3430–3433, doi:10.1109/IGARSS.2016.7729886, 2016.

Stocker, T. F., Qin, D., Plattner, G.-K., Tignor, M., Allen, S. K., Boschung, J., Nauels, A., Xia, Y., Bex, V., Midgley, P. M., et al.: Climate change 2013: The physical science basis, Intergovernmental Panel on Climate Change, Working Group I Contribution to the IPCC Fifth Assessment Report (AR5)(Cambridge Univ Press, New York), 2013.

Stroeve, J., Barrett, A., Serreze, M., and Schweiger, A.: Using records from submarine, aircraft and satellites to evaluate climate model simulations of Arctic sea ice thickness, The Cryosphere, 8, 1–16, doi:10.5194/tc-8-1-2014, 2014.

Stroeve, J. C., Serreze, M. C., Holland, M. M., Kay, J. E., Malanik, J., and Barrett, A. P.: The Arctic's rapidly shrinking sea ice cover: a research synthesis, Climatic Change, 110, 1005–1027, 2012.

Tian-Kunze, X., Kaleschke, L., Maaß, N., Serra, M. M. N., Drusch, M., and Krumpen, T.: SMOS-derived thin sea ice thickness: algorithm baseline, product specifications and initial verification, The Cryosphere, 8, 997–1018, doi:10.5194/tc-8-997-2014, www.the-cryosphere.net/8/997/2014/, 2014.

Tilling, R. L., Ridout, A., Shepherd, A., and Wingham, D. J.: Increased Arctic sea ice volume after anomalously low melting in 2013, Nature Geoscience, 8, 643–646, 2015.

Toudal Pedersen, L., Dybkjær, G., Eastwood, S., Heygster, G., Ivanova, N., Kern, S., Lavergne, T., Saldo, R., Sandven, S., Sørensen, A., and Tonboe, R.: ESA Sea Ice Climate Change Initiative(Sea_Ice_cci): Sea Ice Concentration Climate Data Record from the AMSR-E and AMSR-2 instruments at 25km grid spacing, version 2.0., Centre for Environmental Data Analysis, 28 February 2017, doi:10.5285/c61bfe88-873b-44d8-9b0e-6a0ee884ad95, accessed: 2017-5-30, 2017.

Wadhams, P., III, W. T., Krabill, W., Swift, R., Comiso, J., and Davis, N.: Relationship between sea ice freeboard and draft in the Arctic basin, and implications for ice thickness monitoring, J. Geophys. Res, 97, 1992.

Warren, S. G., Rigor, I. G., Untersteiner, N., Radionov, V. F., Bryazgin, N. N., Aleksandrov, Y. I., and Colony, R.: Snow Depth on Arctic Sea Ice, Journal of Climate, 12, 1814 – 1829, doi:10.1175/1520-0442(1999)012<1814:SDOASI>2.0.CO;2, http://dx.doi.org/10.1175/1520-0442(1999)012<1814:SDOASI>2.0.CO;2, 1999.

Webster, M. A., Rigor, I. G., Nghiem, S. V., Kurtz, N. T., Farrell, S. L., Perovich, D. K., and Sturm, M.: Interdecadal changes in snow depth on Arctic sea ice, Journal of Geophysical Research: Oceans, 119, 5395–5406, doi:10.1002/2014JC009985, http://dx.doi.org/10.1002/2014JC009985, 2014.

Willmes, S. and Heinemann, G.: Pan-Arctic lead detection from MODIS thermal infrared imagery, Annals of Glaciology, 56, 29–37, 2015a.

Willmes, S. and Heinemann, G.: Sea-ice wintertime lead frequencies and regional characteristics in the Arctic, 2003-2015, Remote Sensing, 8, 2015b.

Xu, S., Zhou, L., Liu, J., Lu, H., and Wang, B.: Data Synergy between Altimetry and L-Band Passive Microwave Remote Sensing for the Retrieval of Sea Ice Parameters - A Theoretical Study of Methodology, Remote Sensing, 9, doi:10.3390/rs9101079, 2017.

Zhou, L., Xu, S., Liu, J., Lu, H., and Wang, B.: Improving L-band radiation model and representation of small-scale variability to simulate brightness temperature of sea ice, International Journal of Remote Sensing, 38, 7070–7084, doi:10.1080/01431161.2017.1371862, http://dx.doi.org/10.1080/01431161.2017.1371862, 2017.

Zygmuntowska, M., Rampal, P., Ivanova, N., and Smedsrud, L. H.: Uncertainties in Arctic sea ice thickness and volume: new estimates and implications for trends, The Cryosphere, 8, 705 – 720, doi:10.5194/tc-8-705-2014, www.the-cryosphere.net/8/705/2014/, 2014.

Competing interests. The authors declare no conflict of interest

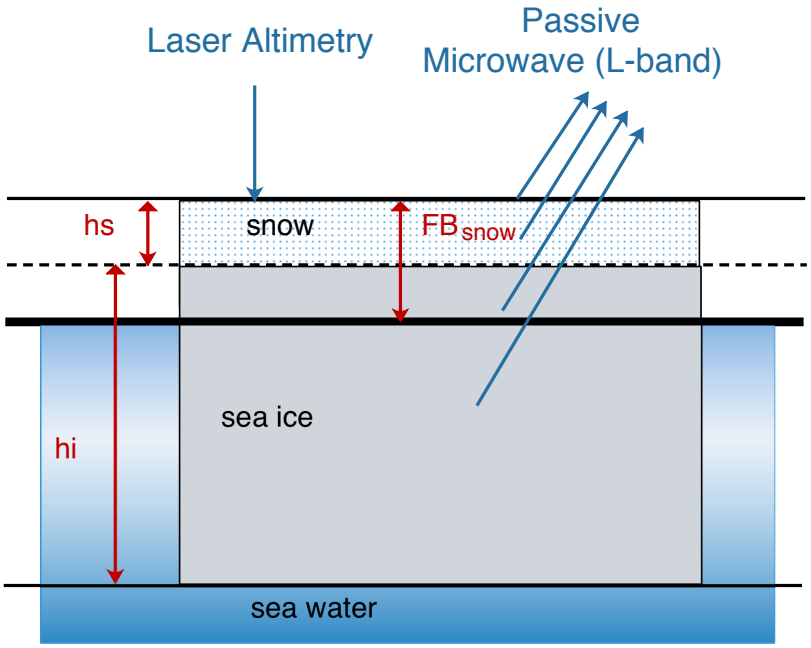

Figure 1. Sea ice parameters in the active and passive remote sensing of the sea ice cover, including sea ice thickness (hi), snow depth (hs) and snow freeboard (FB_s).

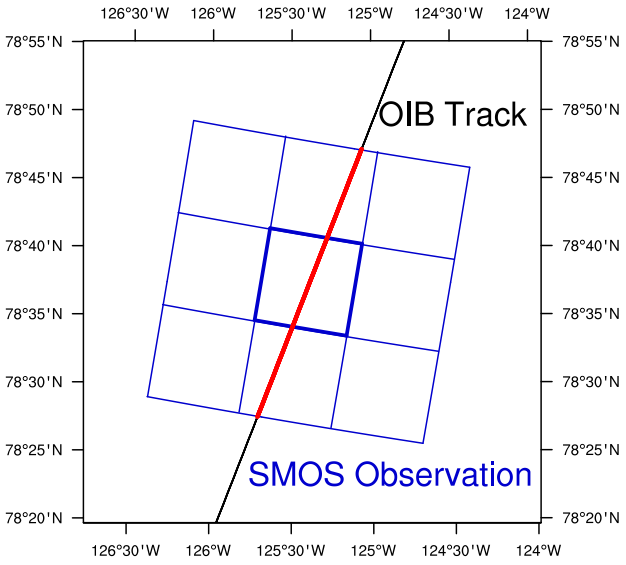

Figure 2. Data match between OIB and SMOS data. SMOS TB product is provided on the 12.5 km EASE grid (shown by blue rectangular cells). However, the inherent resolution of SMOS TB is of about 40 km. The red/black line represents the OIB track. Therefore, in order to accommodate the resolution differences, OIB samples that reside within the 9 cells (red) are considered to be of equal contribution to the TB value at the central EASE grid cell (outline by the thick blue line).

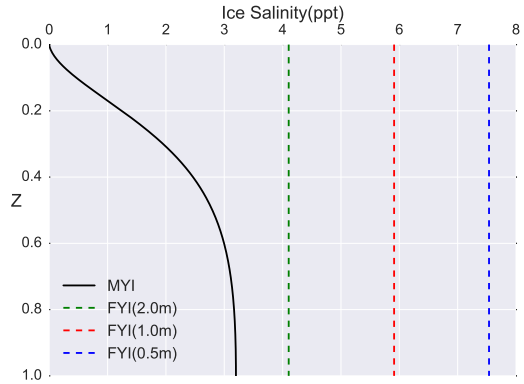

(a) Vertical salinity profile

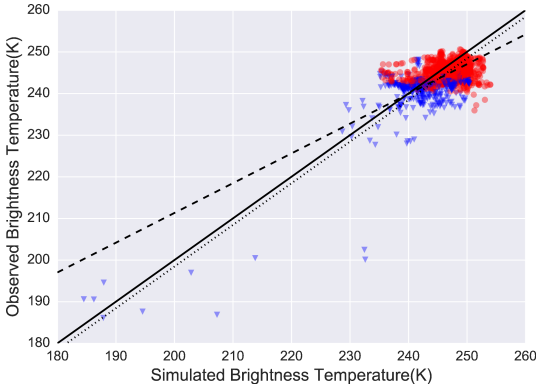

(b) Verification of sea ice radiation model

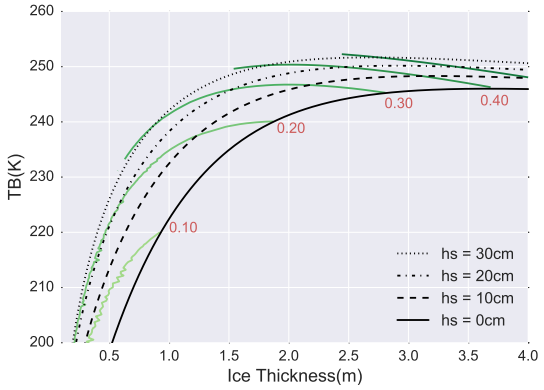

(c) Relationship between TB and sea ice thickness and corresponding FB_s

Figure 3. L-band radiation model. Subfigure a shows sea ice salinity profile for FYI (dotted lines) and MYI (solid line). The vertical axis (Z) is normalized with respect to the sea ice thickness. The comparison of the simulated TB based on OIB data and the observed SMOS TB is presented in subfigure b. Blue triangles represent FYI, while red circles MYI. The dashed (dotted) line is the least squares fit (least squares fit under the constraint that slope be 1). The Root Mean Square Error of TB is 3 K. Subfigure 3 shows the modeled TB under typical parameters (sea ice thickness and snow depth) and sea ice thermal conditions (surface temperature of -30 $^{\circ}C$). The green lines represent constant snow freeboard lines.

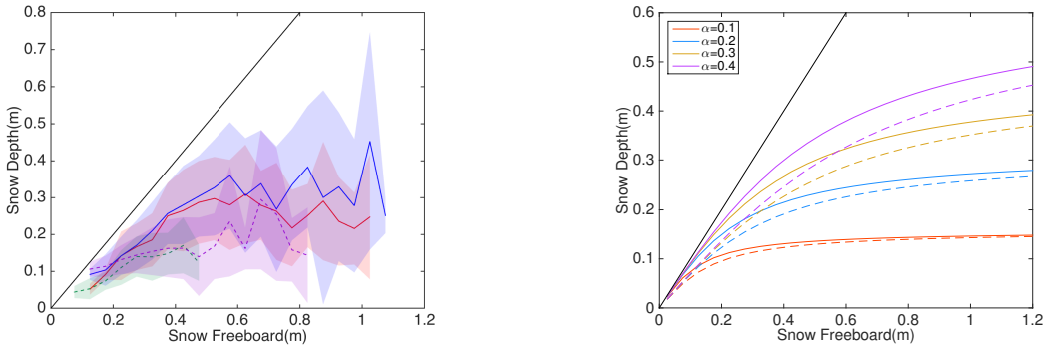

(a) Total freeboard and snow depth

(b) Functional fitting for snow depth

Figure 4. Statistics of snow depth from OIB at the local scale of retrieval. Subfigure a shows the mean and the $+/-1$ standard deviation of the snow depth within each snow freeboard bin (from 0 m to 1.5 m by the interval of 5 cm), shown by lines and shaded areas for 4 realistic cases of OIB. Subfigure b shows the the nonlinear fitting of snow depth over snow freeboard (Equation 3) under representative s values (0.71 for FYI and 0.95 for MYI) and various values of α. Solid color lines are for MYI and dashed ones for FYI. The solid black line is $y = x$.

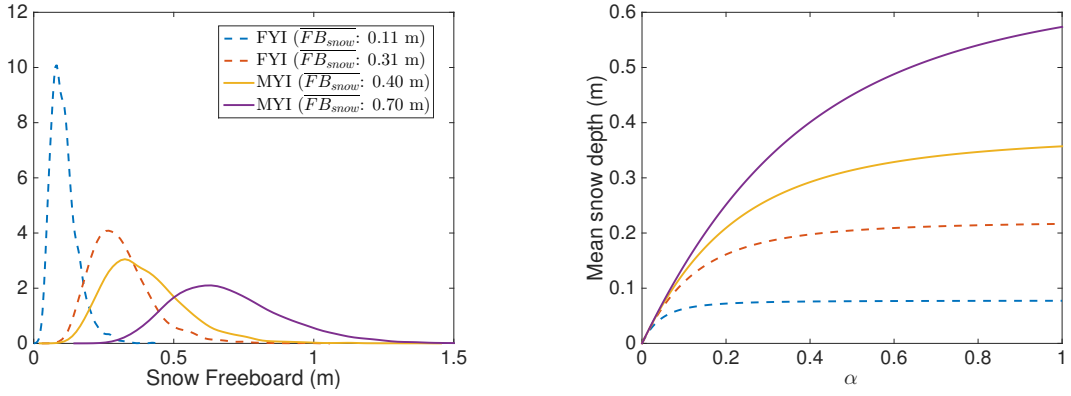

(a) 4 typical distributions of FB_s

(b) Derived mean hs with respect to the values for α

Figure 5. Typical distributions of FB_s and the range of mean hs for $0 < \alpha < 1$. Subfigure a shows the 4 distributions (2 for FYI and 2 for MYI) and the corresponding mean value of FB_s. Global values of s for FYI and MYI are adopted. For these 4 distributions, subfigure b shows the mean hs for the range of α between 0 and 1. Mean hs increases monotonically with α, and saturates when α is large.

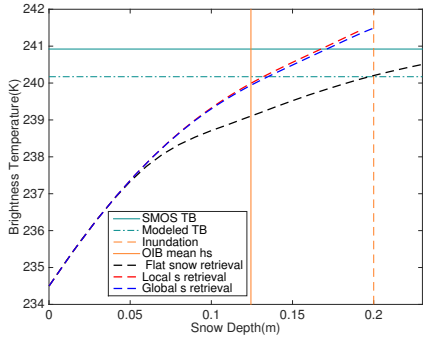

(a) Scenario I

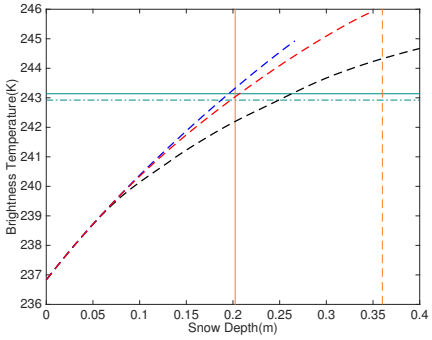

(b) Scenario II

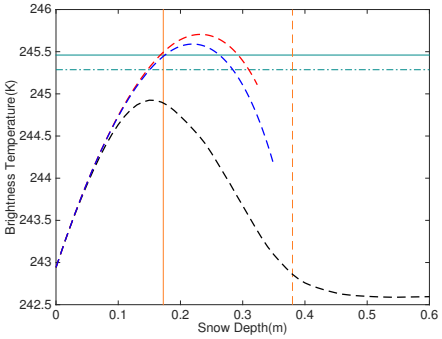

(c) Scenario III

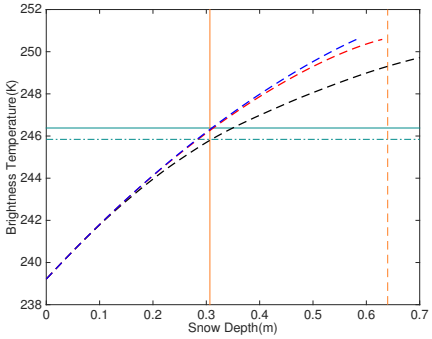

(d) Scenario IV

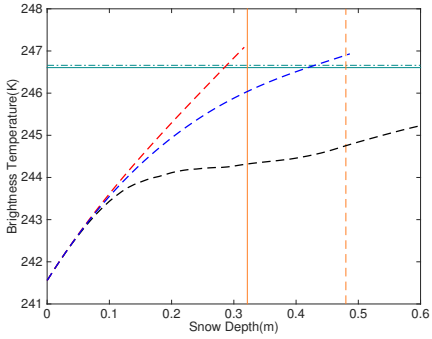

(e) Scenario V

Figure 6. Retrievability study with different retrieval scenarios. The horizontal solid (dotted-dashed) lines are the SMOS (modeled) TB. The vertical solid lines represent the values of the mean snow depth from OIB observation. The black dashed curves denote the values of TB generated by scanning of hs under the flat snow cover assumption, and the vertical dashed lines denote the values of hs that result in 50% OIB samples to be inundated. The red (blue) dashed curves (with the corresponding mean snow depth) are the values of TB generated by scanning of α with the local (global) values of s as in Equation 3.

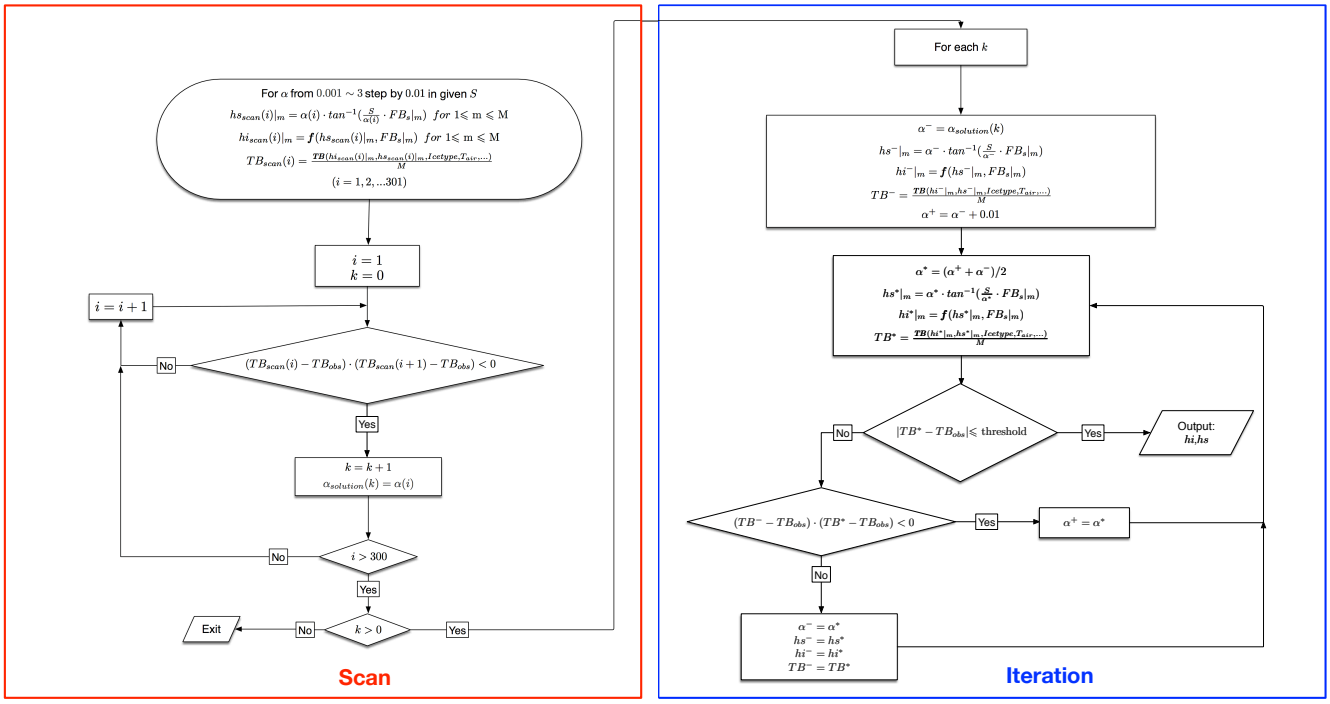

Figure 7. Flow chart for retrieval algorithm. Two phases are marked out. The red box includes the scanning process for the potential solutions to the retrieval problem, and the blue box the iterative binary search for the solving process.

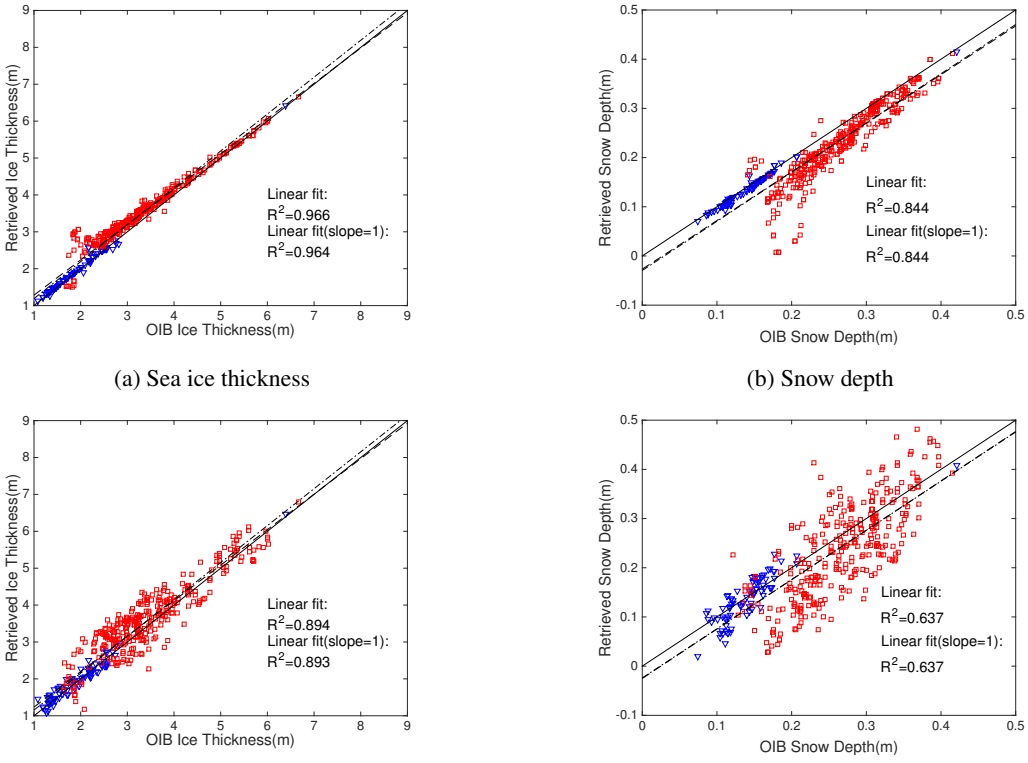

(a) Sea ice thickness

(b) Snow depth

(c) Sea ice thickness

(d) Snow depth

Figure 8. Large-scale retrieval of mean sea ice thickness (subfigure a and c) and mean snow depth (subfigure b and d) and verification with OIB observations. In each subfigure: blue triangles (red rectangles) denote FYI (MYI); the solid line is the 1:1 line; the dashed (dashed dotted) line represents the linear fitting (linear fitting line with the constraint that the slope be 1). The quality of fittings in terms of R^2 are also shown. Subfigure a and b represent the comparison results for the retrieval with modeled TB and the local values of s. Subfigure c and d represent the results with SMOS TB and the global values of s as derived from OIB data.

Table 1. Typical retrieval scenarios. The mean sea ice thickness ($\overline{Hi}$), mean snow depth ($\overline{Hs}$), mean snow freeboard ($\overline{FBs}$), observed TB from SMOS and the simulated TB from forward radiation model are shown. Scenario I and II are FYI, and scenario III, IV and V are MYI.

Ice type	Scenario	$\overline{Hi}\,(m)$	$\overline{Hs}\,(m)$	$\overline{FB_s}\,(m)$	$TB\,(K)$	
					Simulated	Observed
FYI	I	1.28	0.12	0.2212	245.84	246.38
	II	2.25	0.20	0.3790	242.92	243.14
MYI	III	2.46	0.17	0.3807	245.29	245.46
	IV	3.01	0.32	0.5419	246.66	246.61
	V	4.13	0.31	0.6509	245.84	246.38

Table 2. Retrieved results ($\overline{Hs}$ and $\overline{Hs}$, in units of meters) for five scenarios under different retrieval algorithms. In scenario II, IV and V, the retrieval with flat snow cover assumption is unsuccessful. The values in the brackets for scenario V denote the other (possible) solution for sea ice parameters.

Scenario	$\overline{Hi}\ (m)$				$\overline{Hs}\ (m)$			
	Observed	Retrieval w/ flat snow cover	Retrieval w/ local s	Retrieval w/ global s	Observed	Retrieval w/ flat snow cover	Retrieval w/ local s	Retrieval w/ global s
I	1.28	–	0.95	0.93	0.124	–	0.167	0.171
II	2.25	2.00	2.23	2.30	0.202	0.263	0.207	0.195
III	2.46	–	2.50 (1.69)	2.45 (1.88)	0.172	–	0.168 (0.293)	0.175 (0.263)
IV	3.01	–	3.25	2.38	0.321	–	0.285	0.419
V	4.13	3.88	4.09	4.11	0.308	0.350	0.313	0.310